Nanoscale Res Lett (2010) 5:353–359
DOI 10.1007/s11671-009-9487-3

NANO EXPRESS

Fabrication of a Highly Sensitive Chemical Sensor Based on ZnO Nanorod Arrays

Jae Young Park · Sun-Woo Choi · Sang Sub Kim

Received: 24 June 2009 / Accepted: 29 October 2009 / Published online: 18 November 2009
© to the authors 2009

Abstract We report a novel method for fabricating a highly sensitive chemical sensor based on a ZnO nanorod array that is epitaxially grown on a Pt-coated Si substrate, with a top–top electrode configuration. To practically test the device, its O_2 and NO_2 sensing properties were investigated. The gas sensing properties of this type of device suggest that the approach is promising for the fabrication of sensitive and reliable nanorod chemical sensors.

Keywords ZnO nanorod array · Chemical sensor · MOCVD

Recently, nanostructures, such as nanorods and nanowires, made of semiconducting materials have been extensively investigated for the purpose of using their unique properties in various nanoscale functional devices [1, 2]. For instance, ZnO nanostructures have received particular attention due to their many valuable properties and the ease with which ZnO can be made into various nanostructure shapes by many different methods [3–6].

Since nanorods and nanowires have much larger surface-to-volume ratios compared to their thin film and bulk material counterparts, their application to miniaturized highly sensitive chemical sensors has been predicted to be promising [7, 8]. The electrical and chemical sensing properties of single ZnO nanorods have been extensively investigated in recent years by the fabrication and testing of single nanorod field-effect transistors (FETs). According to the results, ZnO nanorods show an *n*-type semiconducting behavior and their electrical transport is strongly dependent on the adsorption and/or desorption nature of chemical species [9–13]. Despite significant achievements in the realization of chemical sensors based on single ZnO nanorods [14–17], there still remain many aspects that should be overcome before their actual application. Firstly, the fabrication of sensors based on individual nanorods involves a careful lithography process in which each fabrication step is expensive and tedious. Secondly, a precise system that can measure currents in the region of 10^{-9} A is necessary to detect the small current changes that occur in a single nanorod during the adsorption/desorption of chemical species. Finally, the slightly different sizes of each nanorod and the different natures of the electrical contacts in each sensor cause poor reproducibility.

In order to overcome the disadvantages of single nanorod chemical sensors, recently the use of vertically aligned nanorod arrays (NRAs) in chemical sensors has been attempted [18–20]. In these works, metal electrodes were simply deposited on top of nanorod arrays using sputtering [18, 20] or aerosol spray pyrolysis [19]. However, this approach is likely to result in not distinctive but gradient interfaces between nanorods and metal electrodes, possibly deteriorating sensor efficiency. Therefore, an approach for fabricating chemical sensors based on ZnO nanorod arrays (NRAs) using more reliable electrode configurations needs to be developed.

In this work, we report a novel approach to fabricating chemical sensors based on ZnO NRAs with a top–top electrode configuration. The approach used a coating and etching process with a photoresist (PR). The results show that the proposed ZnO NRA-based chemical sensor exhibits a comparable sensitivity, a higher reproducibility and can be made in a simpler way, suggesting that the

J. Y. Park · S.-W. Choi · S. S. Kim (✉)
School of Materials Science and Engineering, Inha University, Incheon 402-751, Korea
e-mail: sangsub@inha.ac.kr

proposed approach is promising for fabricating chemical sensors based on ZnO NRAs.

ZnO NRAs were synthesized on Pt-coated Si (001) substrates using a horizontal-type metal organic chemical vapor deposition (MOCVD) system without using any metal catalyst. Pt films of ~120 nm in thickness were deposited on Si (001) substrates by a sputtering method. Before the Pt deposition, a Ti interlayer of ~5 nm in thickness was deposited on the bare Si substrates using the same sputtering method. This was done in order to enhance the adhesion of the Pt films to the Si substrates. According to the high-resolution X-ray diffraction (XRD) results (which are not presented here), the resultant 120-nm-thick Pt films possessed a (111) preferred orientation normal to the substrate plane, while showing a random alignment in the in-plane direction. ZnO NRAs were grown at 500°C for 30 min using O_2 and diethylzinc as precursors with argon as a carrier gas. The pressure in the reactor was kept at 5 torr. The flow rates of the oxygen and diethylzinc were fixed to result in an O/Zn precursor ratio of 68. The microstructures and crystalline quality of the synthesized ZnO NRAs were investigated using field-emission

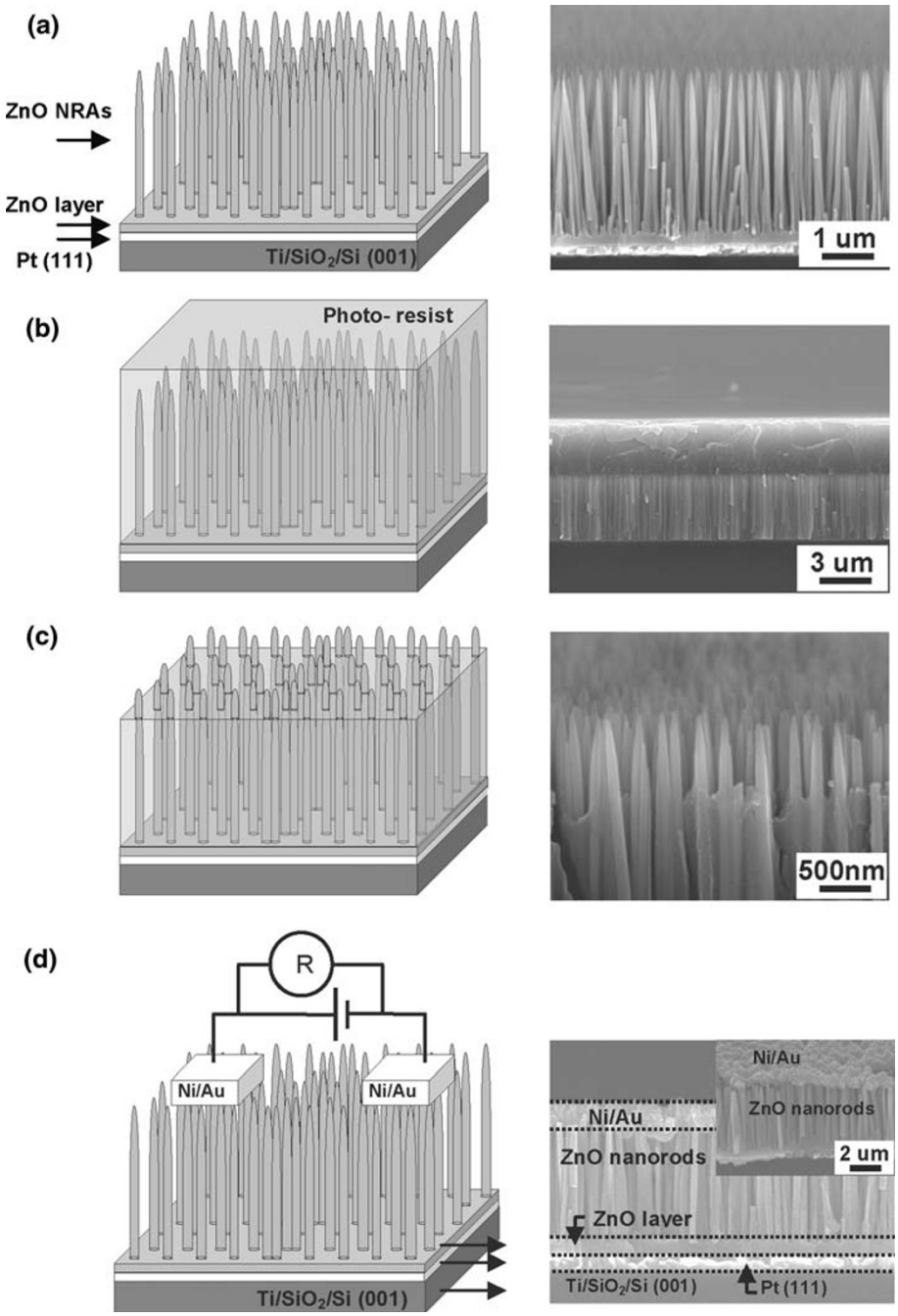

Fig. 1 Schematic (*left*) and real (*right*) images on fabrication of a ZnO NRA sensor. **a** As-synthesized ZnO NRA on a Pt-coated Si (001) substrate. **b** ZnO NRA filled and coated with positive PR. **c** Exposure of the tip-ends of ZnO nanorods by etching with inductively coupled plasma in oxygen atmosphere. **d** Deposition of Ni (~ 500 nm)/Au (~ 50 nm) metal layers by thermal evaporation using a mask and subsequent removal of remaining PR by dipping in acetone. The *inset* in the right part of **d** shows a bird-view of the electrode part

scanning electron microscopy (SEM) and high-resolution transmission electron microscopy (TEM). The growth behavior, alignment nature, substrate dependency, size and shape control, fabrication of the field-effect transistors, and the temperature-dependent electrical transport of the single ZnO nanorods used in this study have been reported in detail in our previous works [21–24].

Figure 1 displays the schematic (left) and real (right) images in sequence on fabrication of chemical sensors in this study using the synthesized ZnO NRAs. The images of an as-synthesized ZnO NRA on a Pt-coated Si (001) substrate are shown in Fig. 1a. For the device fabrication, the NRA was synthesized partly on the substrate using a mask. Positive photoresist (PR) was spread on the surface of the ZnO NRA by a spin coater. As seen in Fig. 1b, a uniform and smooth PR layer was formed. The space between individual ZnO nanorods was completely filled with PR. Next, a small portion of the PR layer was removed by etching with inductively coupled plasma in oxygen atmosphere. This consequently resulted in exposure of the tip-ends of ZnO nanorods (see Fig. 1c). Then, using a mask of 2 mm × 3 mm in area, Ni (~500 nm in thickness) and Au (~50 nm) were sequentially deposited on the exposed tip-ends by thermal evaporation, as shown in Fig. 1d. Finally, the PR filled into the space between nanorods as well as remained on the substrate was removed by dipping into acetone. Then the sample was dried into a vacuum oven at 100°C. Note that the well-defined interface between the nanorods and the electrode layer was formed, as shown in the right part of Fig. 1d. The inset figure shows a bird-view of the electrode part. It shows a continuous, well-defined electrode layer.

As a practical test for ZnO NRA chemical sensor, the sensing properties for O_2 and NO_2 were investigated. The fabricated NRA chemical sensor was introduced into a vacuum chamber equipped with a system that can measure current and voltage by changing O_2 and NO_2 environments using N_2 as a carrier gas. HP 4140B pA Meter/DC voltage source was used as the measurement tool, which was interfaced with a personal computer through a general purpose interface bus (GPIB) card. The chamber pressure was controlled using a gate valve and verified using an ion gauge. The sensor assembly was heated to the desired temperature by using a halogen lamp, and temperature was monitored through a thermocouple. In this study, the sensing measurement was performed at 573 K. The base pressure of the vacuum chamber, which was connected to a turbomolecular pump, was typically $\sim 5 \times 10^{-6}$ torr. Using mass flow controllers, O_2 and NO_2 environments were monitored.

As shown in a field-emission SEM image displayed in Fig. 1, vertically well-aligned ZnO nanorods grew over the Pt/Ti/Si (001) substrate. The nanorods are uniform in diameter and length. It is clear that a continuous ZnO interfacial layer exists. Our previous work on the early growth stages of ZnO nanoneedles on sapphire (0001) revealed that a continuous ZnO layer coherently strained to the substrate grows first [25]. On top of the existing continuous layer, aligned nanoneedles start to form as the growth proceeds further. A similar growth behavior

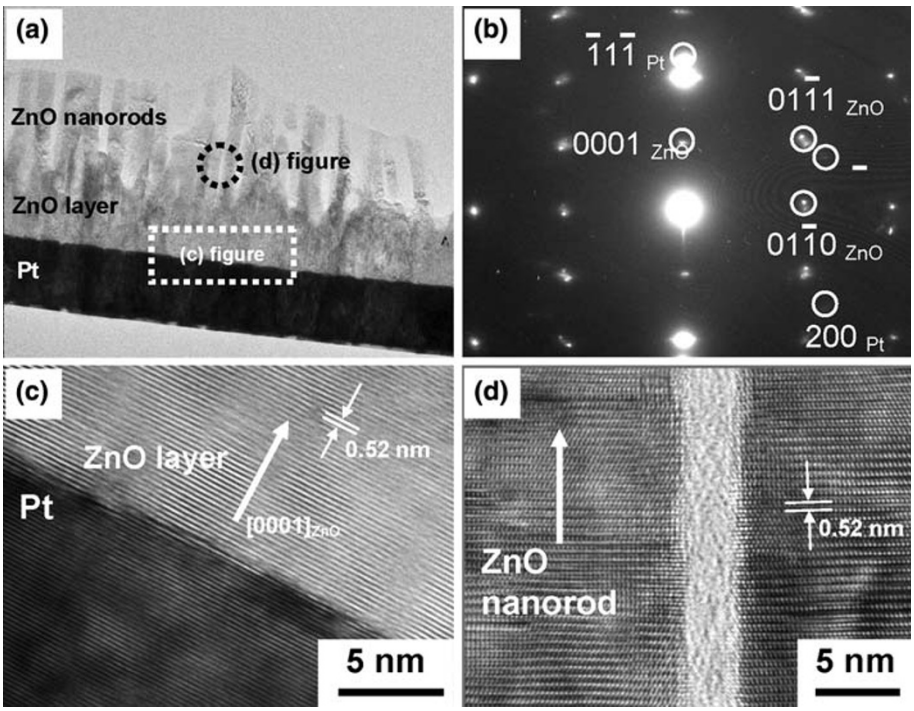

Fig. 2 **a** Bright-field TEM image observed at the interface between a ZnO NRA and a substrate. Note that existence of a continuous ZnO film of 150 nm in thickness on the Pt layer. **b** Selected area electron diffraction pattern taken from a region including the Pt layer, ZnO layer, and ZnO NRA. **c** High-resolution TEM lattice image taken at an interfacial area of the ZnO layer and Pt layer. **d** High-resolution TEM lattice image of individual ZnO nanorods

appears to occur during the growth of the ZnO NRAs on Pt-coated Si substrates. The Ni/Au double layer that is deposited on the tip-ends of the ZnO nanorods shows a well-defined interface and the formation of a continuous layer. To further investigate the microstructure of the ZnO NRAs, TEM studies were carried out.

Figure 2a is a bright-field TEM image taken at the interfacial area between the ZnO NRAs and the substrate. The presence of the ZnO layer is more evident in this image. Figure 2b is a selected area electron diffraction pattern of the ZnO nanorods. This shows their alignment with the (0001) planes parallel to the substrate surface. High-resolution TEM lattice images of the interfacial layer and ZnO nanorods are shown in Fig. 2c, d, respectively. These images show perfect lattice arrays without any considerable dislocations or stacking faults, meaning that the interfacial ZnO layer is of an epitaxial quality and that the individual ZnO nanorods are actually defect-free single crystals.

To practically test the NRA chemical sensor with the top–top electrode configuration, its sensing properties under O_2 and NO_2 environments were investigated. Figure 3a displays the current–voltage (I–V) curves obtained for various O_2 concentrations. Note that for clarity, only some of the results are presented. These I–V curves are linear, indicating ohmic contact nature for the sensing device in O_2 environments. In general, the conductivity in semiconducting oxide sensors shows strong dependency on the oxygen pressure, following the relationship [26]

$$\sigma = A\exp(-E_A/\mathrm{KT})P_{O_2}^{1/m} \quad (1)$$

where σ is the electrical conductance, E_A is the activation energy for atomic diffusion around the grain boundary, A is the pre-exponential factor, K is the gas constant, and T is the temperature in Kelvin. The inset of Fig. 3a shows the plot of log σ versus log P_{O_2}. The slope was $-1/2.85$, indicating that $m = -0.35$. In case of p-type conduction, m is positive. On the other hand, it is negative for n-type conduction. Therefore, n-type conduction is operating in the ZnO NRA at the various O_2 pressures. The value of m relies on the dominating defects related to the sensing mechanism.

The dynamic testing of a sensing device provides useful information about the sensitivity, the response and recovery times, and the reproducibility. Note that as described before, the dynamic testing was performed in the vacuum chamber. Pumping away oxygen or NO_2 has been performed when "gas off" is indicated in Figs. 3, 4, and 5. Figure 3b shows typical response curves of a ZnO NRA chemical sensor to oxygen gas. When the sensor is exposed to oxygen gas, the resistance sharply increases. When the oxygen supply is stopped, the resistance quickly drops to a low value. In order to mention the response and recovery times more clearly, we have to wait for sufficient time and

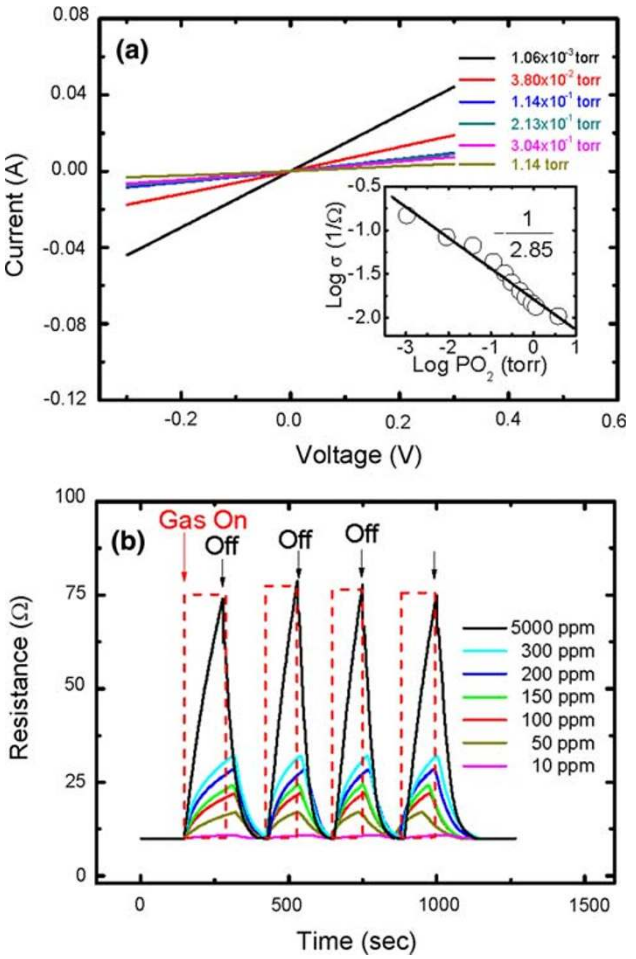

Fig. 3 **a** I–V behavior of a ZnO NRA chemical sensor measured at different O_2 concentrations. The *inset* shows a plot of resistance as a function of O_2 concentration. **b** Typical response curves to various O_2 concentrations

the steady state resistance in oxygen and without oxygen, i.e., saturated state. The resistance curves in Fig. 3b show no saturation. However, the amounts of the resistance change until the initiation of "gas off" were over 90% compared with the saturated values. Thus, although the data show no saturation, it is possible to mention the response and recovery times because they are usually defined as the time required to reach 90% of the final equilibrium value of the sensor signals. Based on this, the response and recovery times were 120–180 and 100–120 s, respectively, depending on the O_2 concentration. It should be noted that the sensor responses were very stable and reproducible for the repeated test cycles. The superior stability and reproducibility come from the fact that the sensing response is the average value from an enormous number of individual nanorods, unlike the sensing response for a single nanorod chemical sensor. For the NRA chemical sensor fabricated with the top–top electrode configuration, considering the total area of the two top

electrodes is 12 mm^2, the diameters of the nanorods are ~100 nm, and the gaps between them are ~100 nm, then ~4×10^8 nanorods participate in the sensing process.

Figure 4a shows the change in resistance as a function of time with different O_2 concentrations ranging from 1.4 to 500 ppm. Six cycles were successively recorded. As shown, the device recovery was reproducible for all O_2 concentrations. The gas sensitivity (S) was estimated using the relationship, $S = ((R - R_0)/R_0)$, where R_0 is the initial resistance in the absence of O_2 gas and R is the resistance measured in the presence of O_2 gas. Figure 4b shows the sensitivities extracted from Fig. 4a as a function of O_2 concentration. The sensitivity at an O_2 concentration of 1.4 ppm is 0.15, which is similar to the values previously reported for oxygen sensors based on single ZnO nanorods [27]. A linear relationship is obtained between sensitivity and O_2 concentration in the O_2 concentration range, as shown in Fig. 4b. The sensitivity of a semiconducting oxide is usually depicted as $S = A[C]^N + B$, where A and B are constants and $[C]$ is the concentration of the target gas or vapor [28]. In the present study, the data fitting results in $S = 0.0059\ [C] + 0.323$ for the NRA chemical sensor. R^2 in the figure represents the quality of the curve fit. Figure 4c shows the dependence of resistance by

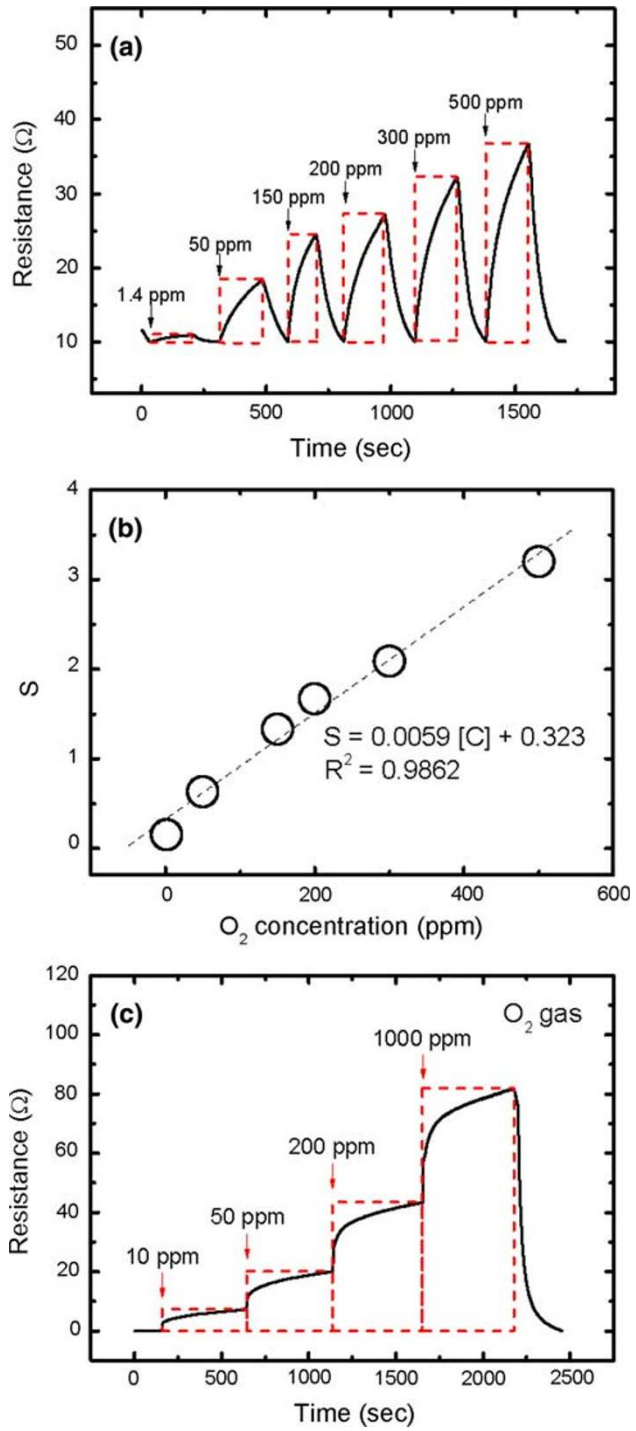

Fig. 4 **a** Resistance change in a ZnO NRA chemical sensor measured at different O_2 concentrations. **b** Sensitivity versus O_2 concentration. **c** Dynamic resistance changes by successive increase in O_2 concentration

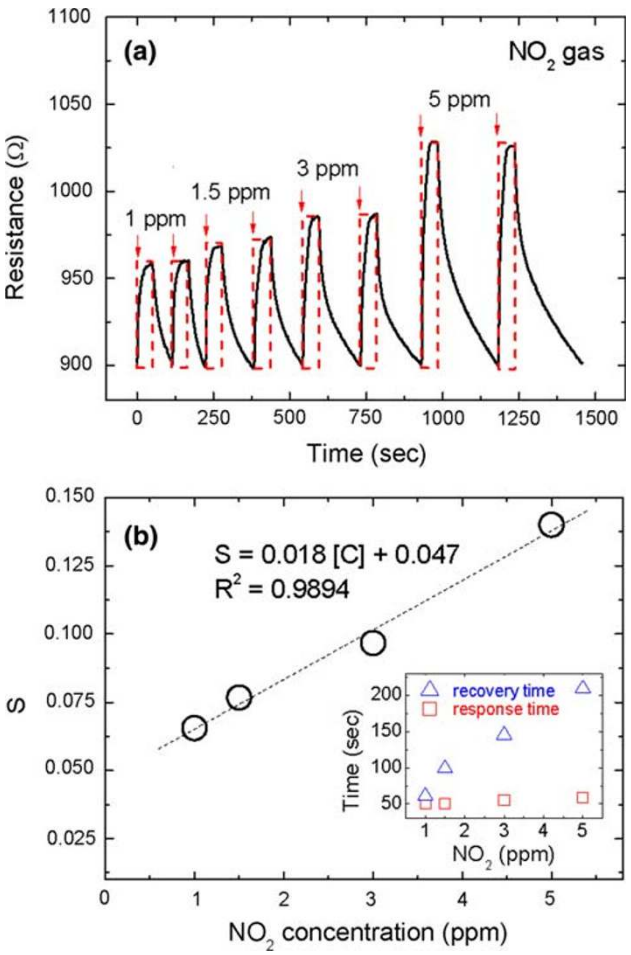

Fig. 5 **a** Resistance change in a ZnO NRA chemical sensor measured at different NO_2 concentrations. **b** Sensitivity versus NO_2 concentration. The *inset* summarizes the response and recovery times with NO_2 concentration

successive increase in O_2 concentration. The resistance quickly responds to the change in O_2 concentration. The increased resistance to O_2 again increases by exposure to more O_2 concentration. This behavior further confirms that the fabricated sensor in this study can be used in the environment with dynamically changing O_2 concentration.

In addition to the O_2 sensing properties of the NRA sensor, its NO_2 sensing properties were investigated. Figure 5a shows the sensing cycles of the NRA sensor measured at 1–5 ppm NO_2. As shown, the sensor well responds to the introduction and removal of NO_2 as low as 1 ppm. The sensitivity of the sensor to NO_2 is summarized in Fig. 5b. The linear slope gives the equation of $S = 0.018\,[C] + 0.047$. The inset of Fig. 5b displays the response and recovery times of the NRA sensor to NO_2 gas of various concentrations. The response time is about 50 s and shows no considerable difference depending on NO_2 concentration. In contrast, the recovery time prolongs from about 55 to 200 s with increasing NO_2 concentration from 1 to 5 ppm. The prolonged recovery time with higher gas concentrations is often observed [29–31].

In case of *n*-type semiconductors like ZnO, oxidizing gas such as O_2 or NO_2 mainly act as an electron accepter in the surface reactions, and the width of electron depletion layers is widened, leading to an increased resistance of the sensors. O_2 or NO_2 molecules adsorbed on the surface of ZnO layers take electrons from them, eventually leading to surface depletion in ZnO. Conversely, the release of electrons occurs in desorption of O_2 or NO_2. This charge transfer accounts for the resistance change observed in the NRA sensor. The sensing results in this study demonstrate that the approach proposed in this study is promising for the fabrication of highly sensitive chemical sensors.

In summary, we have described a novel approach to chemical sensors based on aligned ZnO NRAs grown on Pt-coated Si substrates with a top–top electrode configuration. The O_2 and NO_2 sensing properties of the fabricated sensor showed both a high sensitivity and an excellent reproducibility during the repeated test cycles. The results show that the device proposed in this study is promising for use as a highly sensitive, reliable chemical sensor.

Acknowledgments This work was supported by the Korea Research Foundation Grant funded by the Korean Government (MOEHRD, Basic Research Promotion Fund) (KRF-2008-521-D00177).

References

1. S.-M. Lukas, M.-D. Judith, ZnO–nanostructures, defects, and devices. Mater. Today **10**, 40–48 (2007)
2. Z.L. Wang, Oxide nanobelts and nanowires-growth, properties, and applications. J. Nanosci. Nanotechnol. **8**, 27–55 (2008)
3. G.-D. Yuan, W.-J. Zhang, J.-S. Jie, X. Fan, J.-X. Tang, I. Shafiq, Z.-Z. Ye, C.-S. Lee, S.-T. Lee, Tunable *n*-type conductivity and transport properties of Ga-doped ZnO nanowire arrays. Adv. Mater. **20**, 168–173 (2008)
4. S.Y. Bae, C.W. Na, J.H. Kang, J. Park, Comparative structure and optical properties of Ga-, In-, and Sn-doped ZnO nanowires synthesized via thermal evaporation. J. Phys. Chem. B. **109**, 2526–2531 (2005)
5. D.H. Kim, S.D. Lee, K.K. Kim, G.S. Park, J.M. Lee, S.W. Kim, Free-standing ZnO nanorods and nanowalls by aqueous solution method. J. Nanosci. Nanotechnol. **8**, 4688–4691 (2008)
6. Y.S. Yun, J.Y. Park, H. Oh, J.-J. Kim, S.S. Kim, Electrical transport properties of size-tuned ZnO nanorods. J. Mater. Res. **21**, 132–136 (2005)
7. Q. Wan, Q.H. Li, Y.J. Chen, T.H. Wang, X.L. He, J.P. Li, C.L. Lin, Fabrication and ethanol sensing characteristics of ZnO nanowire gas sensors. Appl. Phys. Lett. **84**, 3654–3656 (2004)
8. Z.L. Wang, FUNCTIONAL OXIDE NANOBELTS: materials, properties and potential applications in nanosystems and biotechnology. Annu. Rev. Phys. Chem. **55**, 159–196 (2004)
9. Q.H. Li, T. Gao, Y.G. Wang, T.H. Wang, Adsorption and desorption of oxygen probed from ZnO nanowire films by photocurrent measurements. Appl. Phys. Lett. **86**, 123117–123119 (2005)
10. X.J. Hung, Y.K. Choi, Chemical sensors based on nanostructured materials. Sens. Actuators B **122**, 659–671 (2007)
11. C.C. Li, Z.F. Du, L.M. Li, H.C. Yu, Q. Wan, T.H. Wang, Surface-depletion controlled gas sensing of ZnO nanorods grown at room temperature. Appl. Phys. Lett. **91**, 032101–032103 (2007)
12. R. Ghosh, M. Dutta, D. Basak, Self-seeded growth and ultraviolet photoresponse properties of ZnO nanowire arrays. Appl. Phys. Lett. **91**, 073108–073110 (2007)
13. Y. Qiu, S. Yang, Nanotetrapods: Controlled vapor-phase synthesis and application for humidity sensing. Adv. Funct. Mater. **17**, 1345–1352 (2007)
14. Z. Fan, J.G. Lu, Gate-refreshable nanowire chemical sensors. Appl. Phys. Lett. **86**, 123510–123512 (2005)
15. K. Keem, J. Kang, C. Yoon, D.-Y. Jeong, B.-M. Moon, S. Kim, Enhanced performance of ZnO nanowire field effect transistors by H_2 annealing. Jpn. J. Appl. Phys. **46**, 6230–6232 (2007)
16. W. Wang, H.D. Xiong, M.D. Edelstein, D. Gundlach, J.S. Suehle, C.A. Richter, Low frequency noise characterizations of ZnO nanowire field effect transistors. J. Appl. Phys. **101**, 044313–044317 (2007)
17. F.V. Farmakis, T. Speliotis, K.P. Alexandrou, C. Tsamis, M. Kompitsas, I. Fasaki, P. Jedrasik, G. Petersson, B. Nilsson, Field-effect transistors with thin ZnO as active layer for gas sensor applications. Microelectron. Eng. **85**, 1035–1038 (2008)
18. H.T. Wang, B.S. Kang, F. Ren, L.C. Tien, P.W. Sadik, D.P. Norton, S.J. Pearton, J. Lin, Hydrogen-selective sensing at room temperature with ZnO nanorods. Appl. Phys. Lett. **86**, 243503–243505 (2005)
19. P. Parthangal, R. Cavicchi, M. Zachariah, A universal approach to electrically connecting nanowire arrays using nanoparticles—application to a novel gas sensor architecture. Nanotechnology **17**, 3786–3790 (2006)
20. J.X. Wang, X.W. Sun, Y. Yang, H. Huang, Y.C. Lee, O.K. Tan, L. Vayssieres, Hydrothermally grown oriented ZnO nanorod arrays for gas sensing applications. Nanotechnology **17**, 4995–4998 (2006)
21. J.Y. Park, D.J. Lee, S.S. Kim, Size control of ZnO nanorod arrays grown by metalorganic chemical vapour deposition. Nanotechnology **16**, 2044–2047 (2005)
22. J.Y. Park, Y.S. Yun, Y.S. Hong, H. Oh, J.-J. Kim, S.S. Kim, Synthesis, electrical and photoresponse properties of vertically

well-aligned and epitaxial ZnO nanorods on GaN-buffered sapphire substrates. Appl. Phys. Lett. **87**, 123108–123110 (2005)
23. J.Y. Park, D.J. Lee, Y.S. Yun, J.H. Moon, B.T. Lee, S.S. Kim, J. Cryst, Temperature-induced morphological changes of ZnO grown by metalorganic chemical vapor deposition. Growth **276**, 158–164 (2005)
24. J.Y. Park, H. Oh, J.-J. Kim, S.S. Kim, The temperature-dependent electrical transport mechanism of single ZnO nanorods. Nanotechnology **17**, 1255–1259 (2006)
25. J.Y. Park, J.M. Lee, J.H. Je, S.S. Kim, J. Cryst, Early stage growth behavior of ZnO nanoneedle arrays on Al_2O_3 (0 0 0 1) by metalorganic chemical vapor deposition. Growth **281**, 446–451 (2005)
26. Y. Xu, X. Zhou, O.T. Sorensen, Oxygen sensors based on semiconducting metal oxides: an overview. Sens. Actuators B **65**, 2–4 (2000)
27. Z. Fan, D. Wang, P.C. Chang, W.Y. Tseng, J.G. Lu, ZnO nanowire field-effect transistor and oxygen sensing property. Appl. Phys. Lett. **85**, 5923–5925 (2004)
28. P.T. Moseley, B.C. Tofield, *Solid State Gas Sensors* (Adam Hilger, Bristol, 1987)
29. F. Naso, F. Babudri, D. Colangiuli, G.M. Farinola, F. Quaranta, R. Rella, R. Tafuro, L. Valli, Thin film construction and characterization and gas-sensing performances of a tailored phenylene−thienylene copolymer. J. Am. Chem. Soc. **125**, 9055–9061 (2003)
30. J. Li, Y. Lu, Q. Ye, M. Cinke, J. Han, M. Meyyappan, Carbon nanotube sensors for gas and organic vapor detection. Nano Lett. **3**, 929–933 (2003)
31. M. Penza, R. Rossi, M. Alvisi, G. Gassano, M.A. Signore, E. Serra, R. Giorgi, Pt- and Pd-nanoclusters functionalized carbon nanotubes networked films for sub-ppm gas sensors. Sens. Actuators B **135**, 289–297 (2008)